Roadmap for Modeling RhPt/Pt(111) Catalytic Surfaces

Jian Zheng,[1]‡ Oleksii Ivashenko,[1]‡ Helmer Fjellvåg,[1] Irene M. N. Groot,[2] Anja O. Sjåstad[1]

[1] Centre for Materials Science and Nanotechnology, Department of Chemistry, University of Oslo, P.O. Box 1033, 0315 Oslo, Norway

[2] Leiden Institute of Chemistry, P.O. Box 9502, 2300 RA Leiden, the Netherlands

ABSTRACT

PtRh alloys are used as versatile multipurpose catalysts for a number of industrial applications, including fertilizer production and ammonia slip catalysts for NO_x abatement purposes. For the latter, ammonia is oxidized to nitrogen at intermediate temperatures. To optimize the PtRh alloyed catalysts and explain the role of Pt and Rh for future intermediate-temperature ammonia oxidation operando studies, we prepared a series of distinct RhPt model surfaces. We explore post-annealing and high-temperature deposition as two routes for preparation of surface alloys, and compare results with literature examples. Scanning tunneling microscopy and X-ray photoelectron spectroscopy provide detailed information on surface morphology and composition, and demonstrate excellent temperature stability of RhPt/Pt(111) in the temperature range targeted for operando catalytic studies. A detailed roadmap summarizes preparation conditions to achieve a broad variety of surface structures.

Introduction

Bimetallic PtRh surfaces are of high importance in heterogeneous catalysis. For instance, rhodium-promoted platinum is essential in industrial high-temperature processes like the Ostwald (NO) and the Andrussow (HCN) processes,[1] and likewise for intermediate-temperature catalytic oxidation of ammonia to nitrogen. In NO_x abatement from exhaust (diesel) combustion engines ammonia (urea) is added to achieve selective catalytic reduction (SCR) with N_2 as the desirable product.[2] State of the art de-NO_x V_2O_5-WO_3/TiO_2 catalysts have an efficiency of 95% at 300 - 400 °C.[3-5] However, SCR technologies with even better efficiency are in progress. One option is to add excess ammonia, which in turn requests a second catalyst downstream, i.e. an ammonia slip catalyst that selectively oxidizes residual ammonia to nitrogen at intermediate temperatures.[6-7] We have shown by means of fixed-bed catalyst performance experiments that supported Pt-, Rh- and bimetallic PtRh nanoparticles (Pt-Rh/Al_2O_3) are well suited for ammonia oxidation at intermediate temperatures.[8] In terms of activity and selectivity to nitrogen, the alloys show different behavior than the monometallic counterparts, Pt and Rh.[8] To the best of our knowledge, the underlying reasons for why the alloyed PtRh nanoparticles perform differently is unknown. Therefore, surface-sensitive experiments to correlate ammonia oxidation product selectivity with PtRh surface composition and structure are called for. In order to perform such studies, well-defined PtRh surfaces are a prerequisite. In this paper, we present a roadmap for the preparation and characterization of well-defined Pt-Rh model catalysts in terms of tailor-made surfaces.

According to the Pt - Rh bulk phase diagram,[9] Pt and Rh (both being cubic closed packing, ccp) form a complete solid solution above 1033 K. Below 1033 K it is proposed, but not confirmed experimentally, that the alloys decompose to a two-phase mixture according to the presence of an immiscibility dome, see ref. [10] and references therein. Small-sized colloidally formed PtRh

nanoparticles exhibit a complete solid solution when simultaneous reduction of the metal salt precursors is facilitated.[11] Finally, in the case of PtRh surfaces, computational modeling suggests that Rh as solute in a Pt host has no tendency to segregate to the surface, whereas the Pt as solute has moderate tendency to segregate from a Rh host.[12] Remarkably, the bulk $Pt_{25}Rh_{75}(110)$ crystal is shown to exhibit strong Pt enrichment of 84% at the surface.[13]

When it comes to PtRh surface alloys, no information is readily available in the literature. The deposition of metal atoms on metal single crystals as e.g. Pt/Pt(111),[14] Rh/Rh(111),[15] Ag/Ag(111),[16] and Ru/Pt(111)[17-18] exhibit similar epitaxial growth patterns, which we will describe through the Pt/Pt(111) system. The morphology of the obtained Pt layer(s) depends strongly on the substrate temperature,[19] presence of impurities[20] and deposition rate. The mobility of Pt atoms on Pt(111)[21] is controlled by a range of barriers for diffusion (terrace, corner, step, intra-layer diffusion) and dissociation (kink, step, dimer dissociation).[22] Owing to the six-fold symmetry of an fcc(111) surface, the formation of a hexagon-like island with six-fold symmetry is expected. In such a hexagon-like island, two types of steps can be distinguished: A and B steps, exhibiting <111> and <100> microfacets, respectively.[23] Both experiments and DFT calculations show that the A and B steps have different free energies of formation and diffusion coefficients along and across the step.[16, 22-25] The consequence of this is that the island shape is extremely sensitive to deposition and annealing temperature. In particular, at lower temperatures one type of facets exhibits faster growth, favoring a corresponding triangular structure with three-fold symmetry.[26] At ca. 500 K, the diffusion coefficient along the two types of steps is equal, both steps advance at the same speed, resulting in an equilibrium hexagonal shape.[26]

Here we report the first study on the nucleation, growth, and alloying properties of nanostructured RhPt/Pt(111) surfaces with a range of diverse morphologies suited for (operando)

catalytic studies by means of near-ambient-pressure X-ray photoelectron spectroscopy (NAP-XPS) and Reactor-scanning tunneling microscopy (STM) (see Figure S1). We explore two routes to obtain alloyed surfaces: post-annealing after room temperature deposition of Rh on Pt(111) and direct Rh deposition at higher temperature. We show that the obtained morphologies depend on the preparation method. Additionally, we investigate the temperature stability of the obtained model surfaces, which is of high relevance for systematic studies of catalyst performance.

Experimental details

The experiments were performed in two setups: an in-house built ReactorSTM at Leiden University[27] and a recently installed commercial ReactorSTM system (Leiden Probe Microscopy B.V., LPM) at the University of Oslo (UiO). The UiO machine is based on the previously reported Leiden ReactorSTM,[27] and contains a preparation and an STM chamber, both with a base pressure of $\sim 1 \times 10^{-9}$ mbar. The preparation chamber allows flexible high-quality sample preparation via Ar^+-sputtering (IQE 11-35, SPECS), vacuum annealing (up to 1300 K), metal deposition through a four-pocket e-beam evaporator (EBE-4, SPECS), and three leak valves for gas co-feeding. Equipment for Auger electron spectroscopy and low-energy electron diffraction (ErLEED 3000D, SPECS) is integrated to evaluate sample purity and crystallinity. The STM chamber is housing an STM system that is capable of scanning from ultrahigh vacuum (UHV) to high pressure (up to 6 bar). The unique design is described in detail by Herbschleb *et al.*[27]

Sample preparation. A Pt(111) single crystal (99.999 %; Surface Preparation Laboratory (SPL), the Netherlands) was cleaned in repetitive cycles of Ar^+-sputtering with an energy of 1 kV for 5 min followed by annealing at 1150 K in both O_2 (10^{-6} mbar, 5 min) and in UHV (5 min). Crystal quality in terms of cleanness, crystallinity, and flatness was verified by means of AES, LEED, and STM. Rhodium was subsequently deposited onto the Pt(111) single crystal using the

e-beam evaporator. The depositions were done at ambient temperature and at selected temperatures in the range from 300 to 700 K. Rh (99.9%, Goodfellow) evaporation was conducted in UHV at a pressure less than 2×10^{-9} mbar, using a flux of 0.05 - 0.08 ML/min for 4 - 15 min, as estimated from STM images. Pt evaporation (99.95%, Goodfellow) was conducted in UHV at a pressure below 2×10^{-9} mbar, using a flux of 0.04 ML/min for 12 min. For studies of the effect of post-annealing, the sample was first prepared at room temperature (RT), then heated to selected temperatures between 400 and 1050 K, kept at the targeted temperature for 5 min, cooled down to RT and investigated using STM.

XPS measurements. XPS analysis was carried out in the ReactorSTM system at Leiden University, which is equipped with a SPECS spectrometer. The monochromatic Al Kα X-rays (1486.6 eV) source was oriented at 54º from the surface normal and electron collection was done along the surface normal. The analyzer pass energy was 10 eV, dwell time 0.1 s. XPS spectra were analyzed using the least-squares curve-fitting program Winspec.[28] Binding energies are reported with an uncertainty of ± 0.1 eV and referenced to the Pt 4f photoemission doublet centered at 71.2 eV, originating from the substrate. Analysis of the Rh 3d spectra included a Shirley baseline subtraction and fitting with a convolution of Gaussian and Lorentzian functions. STM images (not reported) were collected to ensure good correlation between the surfaces studied using XPS at Leiden University and STM at the ReactorSTM at UiO.

STM measurements. Scanning tunneling microscopy was conducted using cut $Pt_{80}Ir_{20}$ 0.25 mm diameter tips (Goodfellow). The CAMERA 4.3 software package developed at Leiden University was used for data recording.[29,30] Imaging was performed in constant current mode at a typical sample bias of −0.5 V and a tunneling current of 0.1 nA.

Particle analysis. Statistics on cluster density, coverage, and height of particles were obtained from STM images using the Gwyddion software package.[31] The Rh surface coverage is reported as total amount of Rh contained in any of the Rh layers, and is estimated by measuring the projected area of the layers. The contribution of the first to third layer was estimated by marking grains with 0.22 and 0.44 nm thresholds, corresponding to heights of one or two atomic layers, respectively.[31]

Results and discussion

Morphology of Rh/Pt(111) as prepared at 300 K

A representative STM image of 0.50 ML Rh deposited on Pt(111) at 300 K is shown in Figure 1a. Rh islands nucleate and grow on the Pt terraces and at the steps uniformly. As can be seen from the line profile (Figure 1b), the height of a Rh single layer (0.22 nm) almost coincides with the height of a Pt step (0.23 nm); i.e. the exact location of a (pure) Pt step is not readily distinguishable at RT. Most of the Rh islands are composed of two layers, sometimes with atoms also present in a third layer. In agreement with this, the height histogram (Figure 1c) has three peaks in intervals of 0.22 nm, corresponding to the three Rh layers, indicating a 3-dimensional growth mode at room temperature. Similarly to Pt/Pt(111),[14] the islands have a nearly triangular shape, pointing in the same direction for both layers, comprising a close packed stacking. We interpret the observation of Rh islands attached to the Pt steps as a possibility of elemental mixing already at 300 K. Depending on the evaporation rate and duration, isolated islands, bridged triangular clusters (as in Figure 1) and networks were formed (see Figure 9).
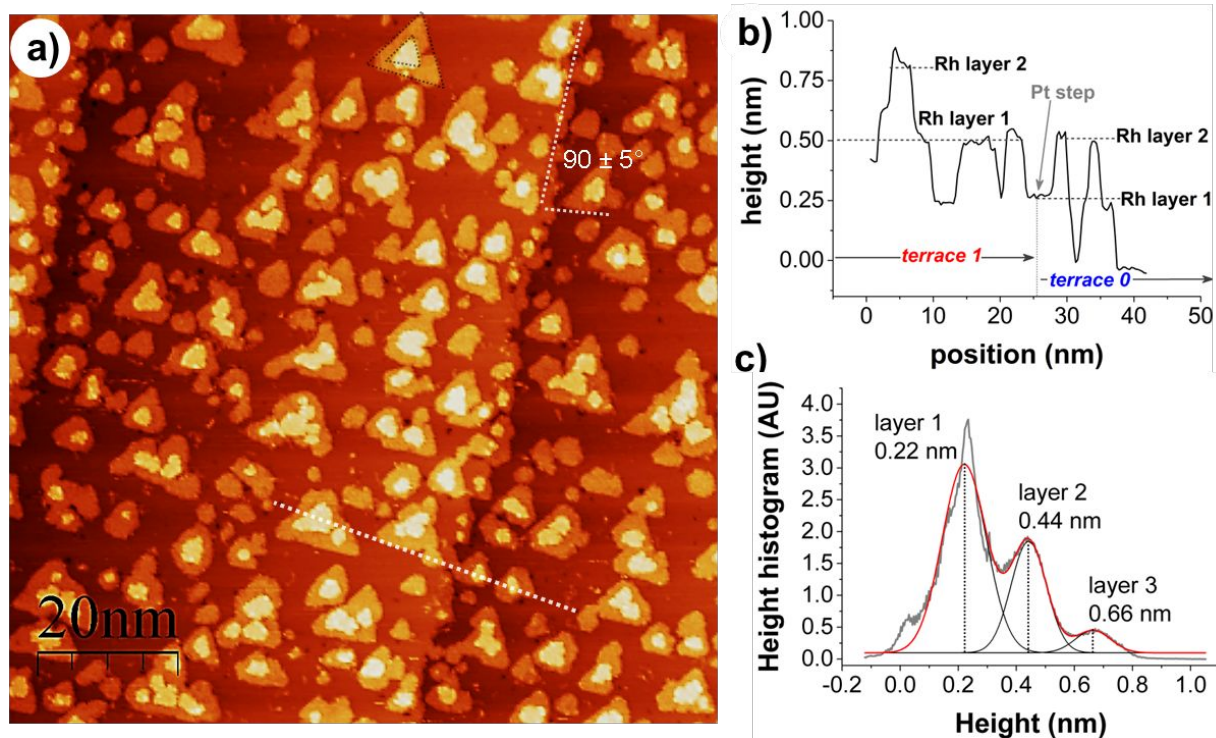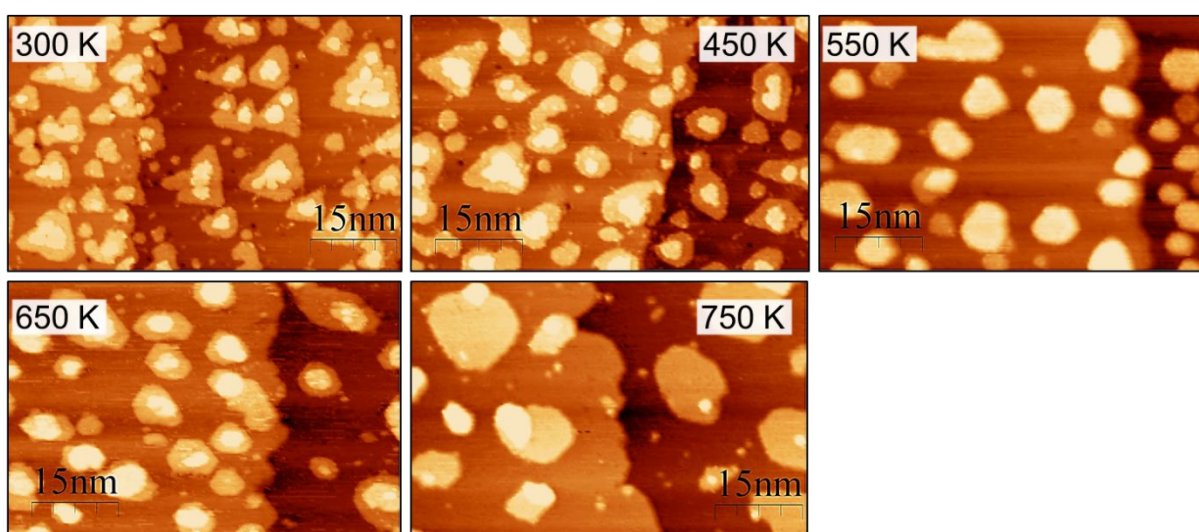
Figure 1. a) STM topography of 0.50 ML Rh on Pt(111) prepared at 300 K, showing homogeneously distributed triangular Rh islands. Dotted line corresponds to the height profile in b). Image size 100×100 nm^2, U_b −0.5 V, I_t 0.1 nA. b) Height profile across the Pt step with Rh islands composed of two layers. The approximate location of a Pt step between terraces 0 and 1 is indicated by an arrow. c) Height histogram showing the presence of three layers with individual height differences of 0.22 nm, measured with respect to Pt terrace level.

Morphology of post-annealed Rh-Pt/Pt(111) surfaces

To mimic commercial and large-surface-area PtRh alloys, model catalyst surfaces[32-36] with a high degree of Rh and Pt mixing are needed. However, for surfaces prepared at 300 K, negligible mixing of Rh at the Pt steps occurs. Hence, to promote inter-diffusion of Pt and Rh at the top layers of the Pt(111) surface, we employed two strategies: i) deposition of Rh at 300 K followed by stepwise post-annealing up to 1050 K; and ii) Rh deposition at elevated temperatures (up to 700 K).

STM images of 0.50 ML Rh on Pt(111) post-annealed at selected temperatures between 450 and 750 K (Figure 2) show significant morphological changes. While annealing at 450 K enabled a minor growth of islands and healing of kinks, annealing at 550 K induced a drastic reshaping of the Rh triangles into hexagons, in which the second layer grew to cover the first one almost fully. Annealing to 650 and 750 K induced further growth and a flattening of the islands, i.e. the second layer decreased in size while adding more material to the first one. The faceting disappeared upon annealing to 900 K, yielding randomly shaped scattered islands (Figure S2).


Figure 2. STM topography of 0.50 ML Rh on Pt(111) flash-annealed to 450 - 750 K and imaged at RT. Triangular clusters grow at 450 K, and transform into hexagons by annealing at 550 - 650 K. Larger single-layered islands are obtained at 750 K. The initially straight Pt steps become roughened due to merging with Rh islands and subsequent alloying. All images are 67×43 nm^2, measured with U_b –0.5 V, I_t 0.1 nA.

Statistical analysis of the data extracted from the STM images for 0.50 ML (Figure 2) and 0.92 ML (Figure S2) of Rh on Pt(111) describes the post-annealing process more quantitatively. The overall island density decreased from 3×10^{12} to 0.63×10^{12} cm^{-2} at 750 K (Figure 3). For the higher starting coverage of 0.92 ML a similar trend is observed, where at 650 K islands merged into

continuous Rh domains (Figure S2). Despite visible morphological changes during post-annealing

of Rh/Pt(111), the apparent coverage of Rh is relatively stable up to 900 K (Figure 3b).

Specifically, the surfaces with 0.50 and 0.92 ML coverage, respectively, at 750 K have lost only

ca. 20% of their initial coverage due to subsurface diffusion. Notably, at and above 550 K, Rh

diffusion into the bulk can be accompanied by Pt diffusing towards the surface, compensating

coverage loss. Thus the coverage estimated from STM may not directly represent the actual surface

composition (see XPS and Pt/Pt(111) results). In addition to interlayer diffusion, the fact that Rh

islands merged with Pt steps is a strong signature of an increased tendency of mixing at elevated

temperature.

   The layer distribution within the islands varied with the annealing temperature (Figure 3c). For

0.50 ML Rh/Pt(111) prepared at 300 K, three layers are distinguishable with populations of 79, 19

and 2%, respectively. At 550 K layer 2 increased two-fold, exhibiting its maximum proportion

(38%), correlating with a minimum for layer 1 (62 %). This suggests that upon annealing to 550

K interlayer diffusion of Rh occurs from layer 1 into layer 2, while subsequent annealing above

550 K drives Rh back into layer 1, which becomes the sole layer above 700 K. The amount of Rh

present in layer 3 can be neglected at post-annealing temperatures above 450 K. A similar behavior

is observed for the 0.92 ML coverage, where two layers remain stable up to 550 K with gradual

transition to single-layer morphology at higher temperatures.
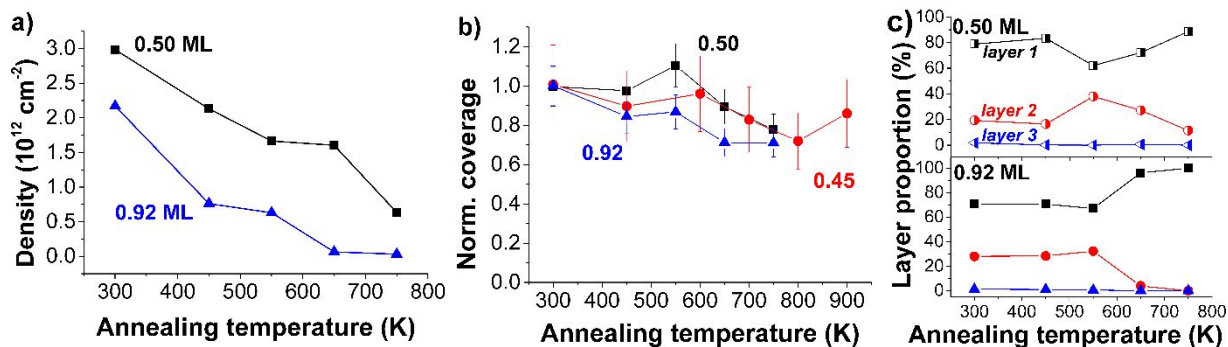
Figure 3. Island statistics as a function of post-annealing temperature estimated from STM images presented in Figure 2 and Figure S2 for 0.50 and 0.92 ML Rh/Pt(111). a) Island density; b) Coverage normalized to as-prepared value at 300 K; c) Proportions of islands deconvoluted into three layers for 0.50 (top panel) and 0.92 ML (bottom panel) Rh/Pt(111).

Composition of post-annealed Rh/Pt(111) surfaces

To extract information on the actual surface composition and possibly induced changes due to post-annealing, XPS spectra were measured for 0.36, 0.55 and 1.00 ML Rh/Pt(111) coverages stepwise flash-annealed up to 1050 K.

For 1.00 ML of Rh/Pt(111) as prepared at 300 K, the Rh $3d_{5/2}$ core level was observed at 306.9 eV,[36] with the Rh 3d$_{3/2}$ partially overlapping with the Pt $4d_{5/2}$ peak at 314.2 eV (Figure 4a). For all coverages post-annealed up to 750 K, the Rh $3d_{5/2}$ binding energy was reproduced at 306.9 eV ± 0.1 eV (Figure S6). To compare several coverages on the same scale we use the intensity ratio of the Rh $3p_{3/2}$ (497 eV) and the Pt $4f$ (71.1 eV) peaks, normalized to the starting Rh/Pt ratio (Figure 4b). Annealing to 550 K led to less than 10% decrease in Rh/Pt ratio, which can be rationalized either by Rh subsurface movement or by onset of Pt incorporation into Rh islands and thus Pt enrichment at the surface. The latter has been reported previously for Ru/Pt(111) deposited at 523 K.[18] This process is further promoted by post-annealing to 750 K, and results in an approximately 20% decrease in the Rh/Pt ratio. Notably, after annealing to 750 K, the STM-based coverage decreased by 25%. Based on this substantial decrease in coverage we conclude that subsurface movement of Rh becomes highly relevant at and above 750 K. Accordingly, with XPS we find a dramatic drop in the Rh signal for 0.55 ML after annealing to 950 (32% remains) and 1050 K (ca. 6% remains).
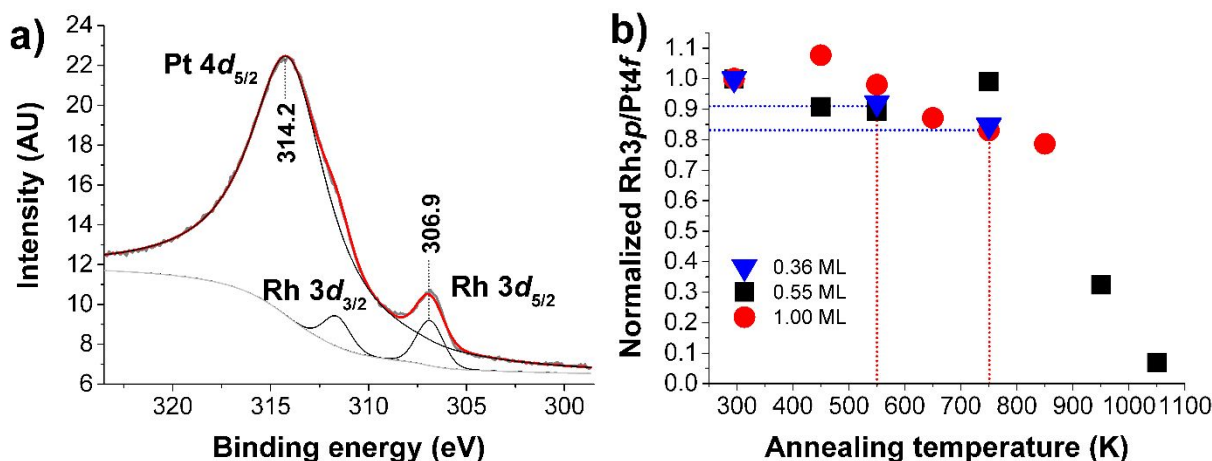
Figure 4. a) X-ray photoelectron spectrum of the Pt $4d_{5/2}$ and Rh $3d$ core levels for 1.00 ML Rh/Pt(111) prepared at 300 K. b) Normalized intensity ratio of the Rh $3p_{3/2}$ peak centered at 497 eV and the Pt $4f$ peak at 71.1 eV as a function of post-annealing temperature for 0.35, 0.55 and 1.00 ML coverages, showing stability of the obtained Rh coverage up to 750 K. Dataset for the sample with 0.55 ML Rh/Pt(111) (black squares) features an outlier at 750 K, attributed to an instrumental factor. Parallel STM measurement showed a decrease in coverage from 0.55 ML to 0.45 ML, i.e. by 18%, as seen for 0.36 ML and 1.00 ML samples.

When combining findings from STM and XPS, we conclude that around 550 K islands acquire an equilibrium hexagonal shape with a significant amount of Rh located in the second layer. This can be facilitated by the onset of Pt diffusion towards the surface, pushing Rh upwards into the second layer. Thereafter, at 550 - 600 K a partial enrichment of the surface with Pt occurs, leading to the formation of a surface alloy, which becomes substantial for surfaces annealed at 650 - 750 K. Thus, we chose to denote the surfaces annealed at and above 550 K not as Rh/Pt(111) but as RhPt/Pt(111). Our results are coherent with the studies of Ru and Pt on Pt(111), which used STM combined with AES to investigate mixing and alloying above 523 K.[18]

Stability of the RhPt/Pt(111) surface at 550 K

It is a prerequisite that a tailor-made nanostructured surface morphology remain stable for the duration time of the operando experiment at relevant temperature conditions for the reaction in question. In this way, one ensures that any observed surface restructuring can be attributed to the presence of gases or adsorbed species. Keeping this in mind, a representative 0.68 ML Rh/Pt(111) surface was prepared at room temperature and flash-annealed at 600 K to promote the equilibrium hexagonal structure and mixing of Rh and Pt within the islands. The subsequent STM image of the RhPt/Pt(111) surface after flash-annealing at 600 K and initial annealing at 550 K for 5 min is shown in Figure 5a, where multiple double-layered hexagons are visible. After additional annealing at 550 K for 2 h (Figure 5b), no significant changes in morphology were observed qualitatively.

To get more quantitative insight, we estimated the coverage after each annealing cycle (Figure 5c). Preparation of the surface using initial flash-annealing to 600 K decreased the Rh coverage from 0.68 to 0.60 ML, in line with the reduction in Rh surface coverage by 10 - 15% after annealing to 550 - 600 K as observed by STM and XPS, see Figure 3 and Figure 4. However, we note some minor differences for the surfaces extensively annealed to 500 K (STM images in Figure S4) and 550 K for 2 - 3 h. Annealing to 500 K resulted in a minor decrease in surface coverage, while annealing to 550 K had no apparent effect or possibly a slight (+0.05 ML) increase in coverage after 3 h. This result can be explained by more facile Pt embedding into Rh islands at 550 K, compensating for minor Rh losses subsurface, as discussed earlier. Overall we conclude that RhPt/Pt(111) does not undergo any significant structural and morphological transformations induced by temperature alone at 550 - 600 K. However, compositional changes in the morphology cannot be ruled out.
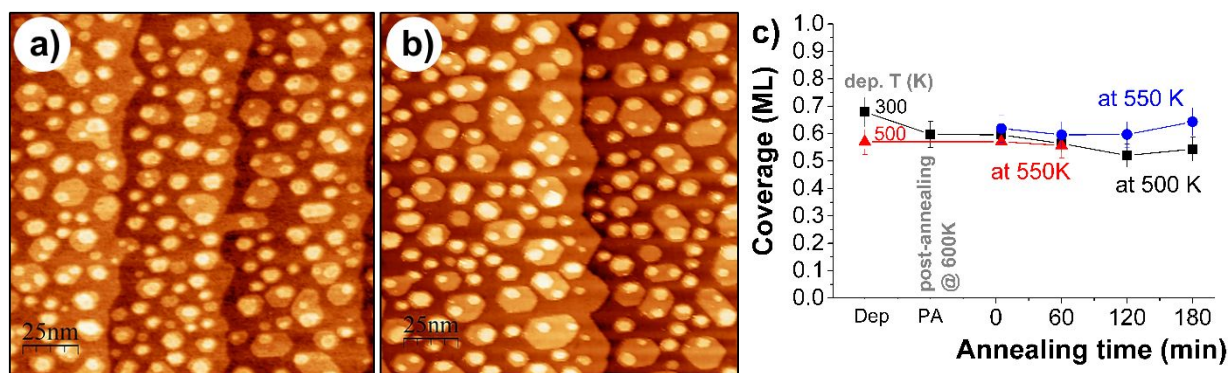
Figure 5. STM topography images of RhPt/Pt(111) prepared at 300 K, flash-annealed at 600 K and annealed at 550 K for 5 min, i.e. before (a) and after (b) extensive heating for 2 h at 550 K. U_b −0.5 V, I_t 0.1 nA. c) Coverage as a function of surface treatment (based on STM). "Dep" and "PA" denote deposition at 300 K and flash annealing at 600 K, respectively. Temperatures for the prolonged annealing are indicated on the graph. Coverage of the sample prepared at 500 K, and heated at 550 K for 1 h is presented for comparison (red line).

Rh deposition at higher temperatures

To promote Rh and Pt mixing and surface alloying to form the RhPt/Pt(111) surface, we explored direct deposition of Rh on Pt(111) at higher temperatures. 0.20 ML of Rh was deposited on Pt(111) kept at 400 - 700 K and imaged after cooling to RT (Figure 6). While the RT deposition of 0.20 ML Rh did not differ from that of 0.50 ML, deposition at 400 K yielded a mixed morphology composed of single-layered triangles, two-layered hexagons, and partially covered two-layered islands with some preference for step decoration. Depositions at 450 and 500 K resulted in formation of larger (25 nm) single- and double-layered triangles pointing in opposite directions (Figure S3). Interestingly, in this temperature range the tendency to nucleate at the Pt steps was further enhanced, manifested in formation of an elongated overlayer along the step. Small nuclei composed of a few atoms were observed in between the Rh islands (note the peak in island density at 450 K in Figure 7c). Deposition at 550 K produced single-layered compact

triangles with sharp edges. At 600 K the islands were shaped into hexagons with slight preferential growth in one direction. At 700 K the STM topography showed an empty surface.
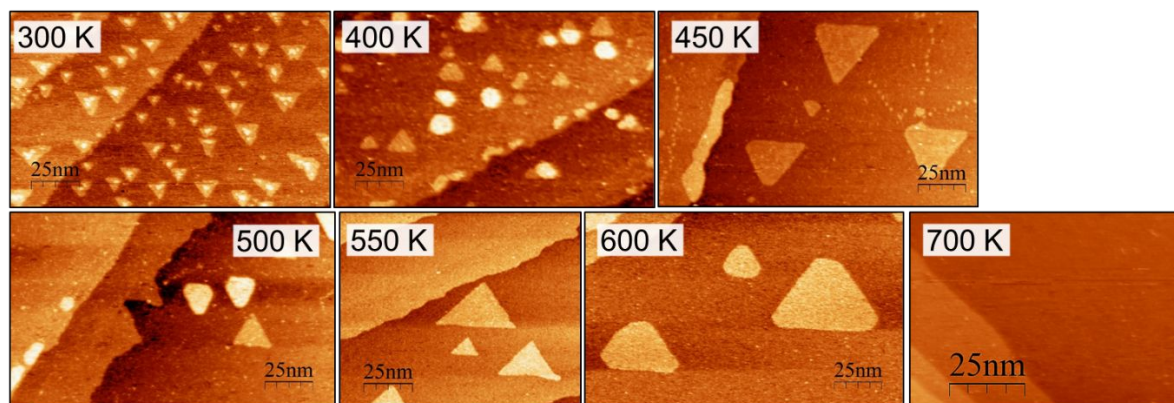

Figure 6. STM topography images of 0.20 ML of Rh deposited on Pt(111) at 300 - 700 K. Measured with U_b −0.5 V, I_t 0.1 nA.
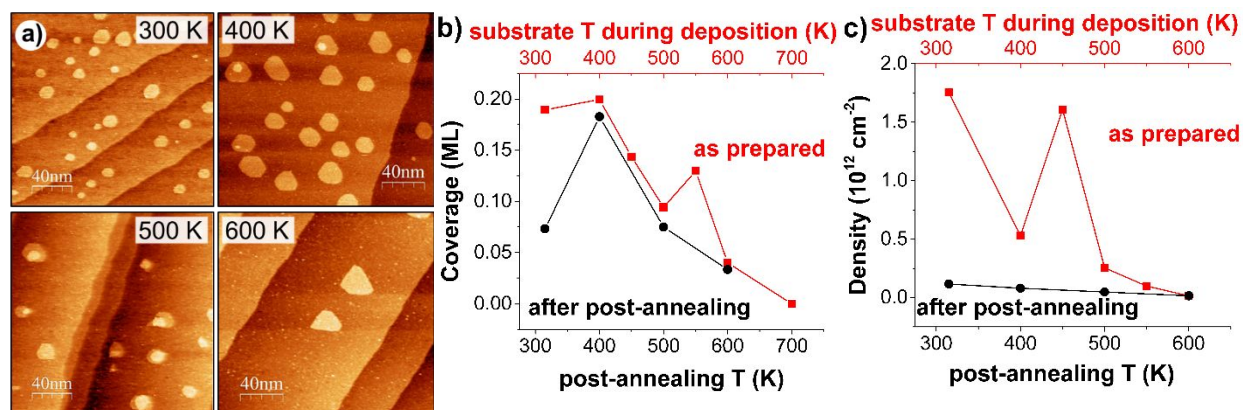

Figure 7. a) STM topography images of 0.20 ML Rh deposited on Pt(111) kept at 300 - 600 K and subsequently flash-annealed to 700 K (deposition temperature indicated in the corner). U_b −0.5 V, I_t 0.1 nA. b) and c) show coverage and island density of as-prepared (red, square) and surfaces (black, circle), after flash-annealing to 700 K, as extracted from STM images in Figure 6 and Figure 7a.

Some more observations should be emphasized. The maximum Rh coverage on steps was found at 450 K. Above 550 K, no overlayers at the steps can be seen, most probably due to subsurface

diffusion of Rh through step channels. At 450 and 500 K no significant subsurface diffusion of Rh into Pt on terraces occurs, based on observation of small nuclei trapped on the surface between Rh clusters (Figure S3), which disappear above 550 K.

Finally, to compare morphologies obtained at elevated growth temperatures with those obtained using post-annealing (Figure 3), a selection of the surfaces imaged in Figure 6 were flash-annealed to 700 K (Figure 7). In general, for depositions originally at 300 - 600 K, with subsequent flash annealing to 700 K the shape of all islands changed to hexagon-like. The islands varied in size around 10 - 30 nm. The most well-defined hexagons with also a narrow size distribution were obtained for surfaces prepared at 400 K and flash annealed to 700 K. As expected for post-annealing, island density decreased substantially with the most significant change evident for samples post-annealed after deposition at 300 - 400 K (Figure 7c). Preparation of surfaces above 450 K results in a significantly lower Rh coverage (75% of that at RT, and dropping down ($< 50\%$) as the deposition temperature increases further), which implies that adatoms have less time to form (or join) a critical nucleus before diffusion subsurface occurs. This effect is expected to be particularly pronounced at the low evaporation rates (0.05 ML/min) employed in this study.

Comparison with post-annealed Pt/Pt(111)

To compare the morphology of post-annealed Rh/Pt(111) and post-annealed Pt/Pt(111) we deposited 0.38 ML Pt on Pt(111) at 300 K and flash-annealed at 450 - 750 K (Figure 8).
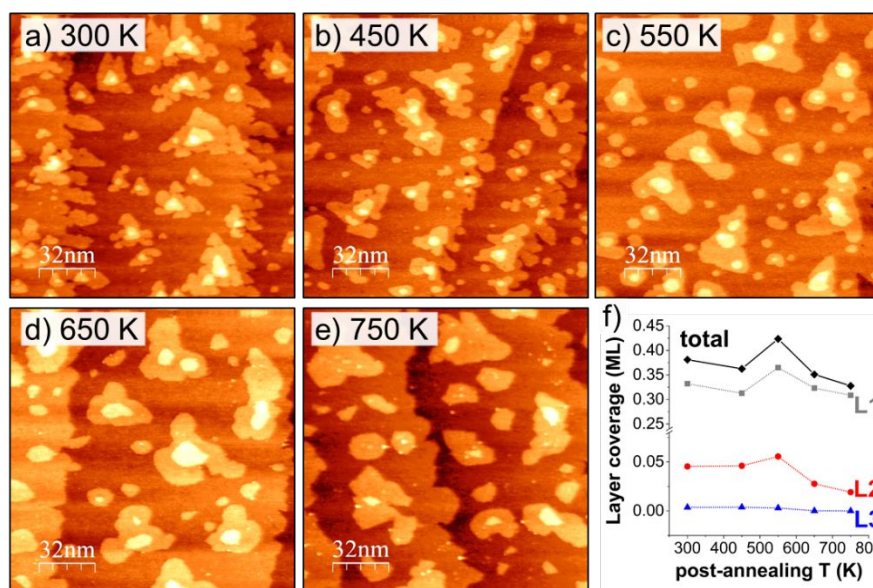
Figure 8. a - e) STM topography images of 0.38 ML Pt deposited on Pt(111) at 300 K and post-annealed to 450 - 750 K for 5 min. Image size 160×160 nm^2, U_b −0.5 V, I_t 0.1 nA. f) Coverage of layers 1 - 3 obtained from STM images in a - e).

Consistent with literature,[14] at 300 K Pt grows into 3D triangle-like structures with all three layers pointing in the same direction. Similarly to Rh/Pt(111), step-wise annealing to 750 K causes island growth, resulting in a steady decrease in cluster density. Notably the third layer, formed at 300 K, contributing only to ca. 1% of the total coverage, remains on the surface up to 550 K and vanishes after annealing at 650 K. Similar to the evolution of the layers for 0.50 ML Rh/Pt(111) in Figure 3, post-annealing of Pt/Pt(111) to 550 K results in a slight growth of the second layer (Figure 8f). More interesting, the first layer exhibits a more pronounced increase in the coverage after annealing at 550 K. Thus, summarizing the contributions from all three layers, at 550 K the coverage of 0.42 ML is 10% higher than the starting coverage, and 17% higher than the coverage at 450 K. Subsequent annealing to higher temperatures causes a decrease in coverage from 0.42 to 0.33 ML (−13% relative to starting coverage). The increase in total coverage for both Rh/Pt(111) and Pt/Pt(111), Figure 3b and Figure 8f, respectively, is attributed to diffusion of Pt atoms into

existing Rh and Pt islands. Annealing to higher temperatures allows atoms from the second or third layer to diffuse down into the first layer, and furthermore into the Pt(111) crystal.

Roadmap for preparing RhPt/Pt(111) surfaces

The deposition and annealing of Rh on Pt(111) employing various experimental conditions gave rise to a variety of island morphologies as summarized in the roadmap, Figure 9. Starting from deposition at room temperature, the major effects of post-annealing are cluster growth, shape transformation from triangular to hexagonal, and intermixing of Rh and Pt at steps and terraces (Figure 9, middle panel). As illustrated in Figure 2 and Figure S2, annealing of RT-deposited samples above 550 K is sufficient for formation of hexagon-shaped structures. In contrast, such hexagon-shaped islands are never directly obtained by high temperature deposition of Rh on Pt kept at 550 - 600 K, but only via subsequent post-annealing (Figure 7). We also find that room temperature deposition combined with post-annealing yields more stable islands, which loose less than 20% of the Rh signal at 700 K as indicated by XPS data. This is in striking contrast to high-temperature deposition, where at 700 K no Rh overlayer was found at the surface, and already at 550 K the island coverage dropped by 50% (Figure 3b and Figure S4). Furthermore, morphologically the post-annealed samples are quite stable (at least 3 h at 550 - 600 K) in UHV, which is a prerequisite for systematic studies.
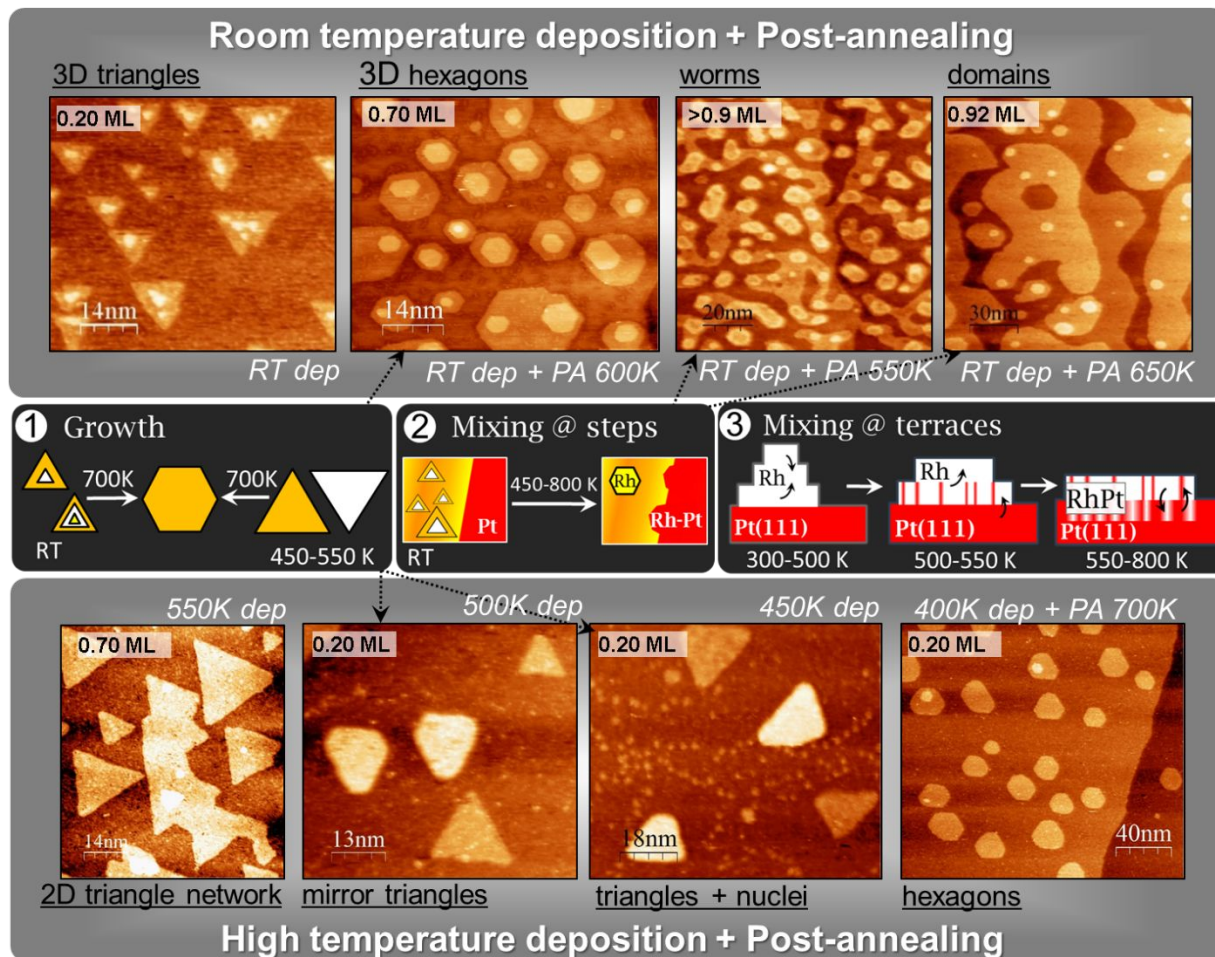
Figure 9. Roadmap for achieving distinct alloyed RhPt morphologies on Pt(111) using post-annealing (top panel) and deposition at higher temperatures (bottom panel). Structures like 3D triangles and hexagons, worms, domains, 2D networks, opposing triangles, small nuclei, and 2D hexagons can be prepared at the indicated conditions (white font). The starting Rh coverage as estimated by STM is indicated for each surface.

For mimicking a working Pt-Rh alloyed catalyst it is crucial that the two elements form a solid solution in the model material, specifically, that a surface alloy RhPt/Pt(111) exists. We found that post-annealing to 600 K or deposition above 550 K are needed to induce such mixing of Pt and Rh. The mixing takes place within the islands, on terraces and step edges (Figure 9, middle panel).

In the context of alloying within the island, it is important to mention that Pt detachment from the Pt step edges and self-diffusion to reach an adjacent Rh island can occur within the temperature range studied. In particular, it could explain a small increase in STM-based coverage at 550 K (**Figure 3** and **Figure 8**). In contrast, data for the post-annealing to higher temperatures does not support this, where no additional coverage due to Pt enrichment arriving from the step edges was observed. The presence of islands on top of the step edges, complete islands merged with steps and denuded areas adjacent to the edges was interpreted as tendency to mix with the step without additional Pt laterally diffusing from the step.

Near surface alloy (NSA) in which Rh island would reside underneath the first layer of Pt was suggested in the literature and at lower temperature it can be excluded based on 3-dimensional growth of islands. Formation of NSA may be more likely at elevated temperatures, where 2-d growth is observed, however our preliminary STM imaging with chemical contrast does not support this hypothesis. STM image obtained after adsorbate-induced tip switching (Figure S5), similarly to Varga et al.,[13] shows that single layer with uniform topography in fact features a complex surface alloy structure when imaged with chemical contrast.

Obtaining alloying of Pt and Rh in these nanostructures upon gentle annealing is in line with what is known for PtRh-based nanoparticles in supported catalysts, and in consensus with predictions of Ruban *et al*. for Pt-Rh surfaces.[12] With reference to this work, we expect that Rh mixes with Pt as RhPt/Pt(111).

Conclusions

Rhodium evaporated onto Pt(111) surfaces was shown to acquire a number of different morphologies, which were controlled via the preparation parameters – coverage, deposition rate, substrate temperature during deposition, and post-annealing. Structures that resemble triangles, triangular networks, worms, hexagons, and domains with hexagon vacancies were obtained. The access to a large number of island shapes and compositions is particularly useful for establishing structure-performance relationships. The observed morphology and (Rh island – Pt surface) mixing is qualitatively similar to the archetypical system of Pt homoepitaxially grown on Pt(111) [14, 20, 26] and heteroepitaxial examples of Ru/Pt(111), [17-18] and is governed by a combination of inter- and intra-layer diffusion barriers.

For future studies of intermediate-temperature ammonia oxidation, we developed a recipe employing post-annealing and high temperature deposition, which resulted in well-mixed RhPt surfaces with either triangular or hexagonal island shapes. The optimal window for Rh and Pt mixing is found around 550 ± 50 K, which allows Rh diffusion into the top layers of the Pt(111) crystal, and Pt diffusion into Rh islands. The post-annealed surfaces exhibited very good temperature stability and maintained their initial morphology for at least 3 h without evidence of sintering or diffusion subsurface at 550 - 600 K.

In terms of morphologies and degree of mixing, the distinct nano-structuring obtained by manipulating the steps in the preparation routes is expected to result in marked differences in catalytic activity and selectivity. Hence, we foresee these surfaces to become particularly useful in systematic studies to optimize Pt-Rh alloying for catalysis.

ASSOCIATED CONTENT

Supporting Information. Detailed description of the experimental setup *ReactorSTM*, additional STM images and XPS spectra are included in the online supporting information. The following files are available free of charge.

Supporting information (PDF).

AUTHOR INFORMATION

Corresponding Author

Anja O. Sjåstad, a.o.sjastad@kjemi.uio.no

Author Contributions

The manuscript was written through contributions of all authors. All authors have given approval to the final version of the manuscript. ‡These authors contributed equally.

REFERENCES

1. Hagen, J., *Industrial Catalysis: A Practical Approach*. Wiley-VCH Verlag GmbH & Co. KGaA: Weinheim, Germany, 2015.

2. Skalska, K.; Miller, J. S.; Ledakowicz, S., Trends in Nox Abatement: A Review. *Sci. Total Environ.* **2010,** *408*, 3976-3989.

3. Lietti, L.; Alemany, J. L.; Forzatti, P.; Busca, G.; Ramis, G.; Giamello, E.; Bregani, F., Reactivity of V_2O_5-WO_3/TiO_2 Catalysts in the Selective Catalytic Reduction of Nitric Oxide by Ammonia. *Catal. Today* **1996,** *29*, 143-148.

4. Guan, B.; Zhan, R.; Lin, H.; Huang, Z., Review of State of the Art Technologies of Selective Catalytic Reduction of Nox from Diesel Engine Exhaust. *Appl. Therm. Eng.* **2014,** *66*, 395-414.

5. Jansson, J., Vanadia-Based Catalysts for Mobile Scr. In *Urea-Scr Technology for Denox after Treatment of Diesel Exhausts*, Nova, I.; Tronconi, E., Eds. Springer: New York, 2014; pp 65-96.

6. Johnson, T. V., Review of Selective Catalytic Reduction (Scr) and Related Technologies for Mobile Applications. In *Urea-Scr Technology for Denox after Treatment of Diesel Exhausts*, Nova, I.; Tronconi, E., Eds. Springer: New York, 2014; pp 3-31.

7. Jabłońska, M.; Palkovits, R., Copper Based Catalysts for the Selective Ammonia Oxidation into Nitrogen and Water Vapour—Recent Trends and Open Challenges. *Appl. Catal., B: Env.* **2016,** *181*, 332-351.

8. Dhak, P. M., M.M.; Bundli, S.A.; Jensen, M.; Zacharaki, E.; Fjellvåg, H.; Menon, M.; Skau, K.I.; Warner, M.; Waller, D.; Sjåstad, A.O., In *Monodisperse Bimetallic Pt-Rh and Pt-Pd Nanoparticles for Intermediate Temperature Ammonia Oxidation*, 17th Nordic Symposium on Catalysis, Lund, Sweden, June 14-16, 2016; Lund, Sweden, 2016.

9. Massalski, T. B.; Okamoto, H.; Subramanian, P. R.; Kacprzak, L., *Binary Alloy Phase Diagrams*. 2nd ed.; ASM International: Ohio, USA, 1990.

10. Steiner, C.; Schönfeld, B.; Portmann, M. J.; Kompatscher, M.; Kostorz, G.; Mazuelas, A.; Metzger, T.; Kohlbrecher, J.; Demé, B., Local Order in Pt-47 At. % Rh Measured with X-Ray and Neutron Scattering. *Phys. Rev. B.* **2005,** *71*, 104204.

11. Park, J. Y.; Zhang, Y.; Grass, M.; Zhang, T.; Somorjai, G. A., Tuning of Catalytic Co Oxidation by Changing Composition of Rh−Pt Bimetallic Nanoparticles. *Nano Lett.* **2008,** *8*, 673-677.

12. Ruban, A. V.; Skriver, H. L.; Nørskov, J. K., Surface Segregation Energies in Transition-Metal Alloys. *Phys. Rev. B.* **1999,** *59*, 15990-16000.

13. Hebenstreit, E. L. D.; Hebenstreit, W.; Schmid, M.; Varga, P., Pt25rh75(111), (110), and (100) Studied by Scanning Tunnelling Microscopy with Chemical Contrast. *Surf. Sci.* **1999,** *441*, 441-453.

14. Bott, M.; Michely, T.; Comsa, G., The Homoepitaxial Growth of Pt on Pt(111) Studied with Stm. *Surf. Sci.* **1992,** *272*, 161-166.

15. Tsui, F.; Wellman, J.; Uher, C.; Clarke, R., Morphology Transition and Layer-by-Layer Growth of Rh(111). *Phys. Rev. Lett.* **1996,** *76*, 3164-3167.

16. Freund, J. E.; Edelwirth, M.; Grimminger, J.; Schloderer, R.; Heckl, W. M., Stm-Induced Formation of Ag Islands on Ag(111). *Appl. Phys. A* **1998,** *66*, S787-S790.

17. Bergbreiter, A.; Berko, A.; Erne, P. M.; Hoster, H. E.; Behm, R. J., On the Origin of Ru Bilayer Island Growth on Pt(111). *Vacuum* **2009,** *84*, 13-18.

18. Berkó, A.; Bergbreiter, A.; Hoster, H. E.; Behm, R. J., From Bilayer to Monolayer Growth: Temperature Effects in the Growth of Ru on Pt(111). *Surf. Sci.* **2009,** *603*, 2556-2563.

19. Bott, M.; Hohage, M.; Michely, T.; Comsa, G., Pt(111) Reconstruction Induced by Enhanced Pt Gas-Phase Chemical Potential. *Phys. Rev. Lett.* **1993,** *70*, 1489-1492.

20. Kalff, M.; Comsa, G.; Michely, T., How Sensitive Is Epitaxial Growth to Adsorbates? *Phys. Rev. Lett.* **1998,** *81*, 1255-1258.

21. Bassett, D. W.; Webber, P. R., Diffusion of Single Adatoms of Platinum, Iridium and Gold on Platinum Surfaces. *Surf. Sci.* **1978,** *70*, 520-531.

22. Jacobsen, J.; Jacobsen, K. W.; Nørskov, J. K., Simulations of Homoepitaxial Growth of Pt(111): Island Shapes and the Growth Mode. *Scanning Microsc.* **1998,** *12*, 81-91.

23. Lundgren, E.; Schmid, M.; Leonardelli, G.; Hammerschmid, A.; Stanka, B.; Varga, P., On the Role of Kinks and Strain in Heteroepitaxial Growth: An Stm Study. *Surf. Rev. Lett.* **2000,** *07*, 673-677.

24. Lundgren, E.; Stanka, B.; Leonardelli, G.; Schmid, M.; Varga, P., Interlayer Diffusion of Adatoms: A Scanning-Tunneling Microscopy Study. *Phys. Rev. Lett.* **1999,** *82*, 5068-5071.

25. Jacobsen, J.; Jacobsen, K. W.; Nørskov, J. K., Island Shapes in Homoepitaxial Growth of Pt(111). *Surf. Sci.* **1996,** *359*, 37-44.

26. Michely, T.; Hohage, M.; Bott, M.; Comsa, G., Inversion of Growth Speed Anisotropy in Two Dimensions. *Phys. Rev. Lett.* **1993,** *70*, 3943-3946.

27. Herbschleb, C. T.; van der Tuijn, P. C.; Roobol, S. B.; Navarro, V.; Bakker, J. W.; Liu, Q.; Stoltz, D.; Cañas-Ventura, M. E.; Verdoes, G.; van Spronsen, M. A., et al., The Reactorstm: Atomically Resolved Scanning Tunneling Microscopy under High-Pressure, High-Temperature Catalytic Reaction Conditions. *Rev. Sci. Instrum.* **2014,** *85*, 083703.

28. *Least-Squares Curve Fitting Program Winspec*, 2.09; LISE laboratory of the Facultes Universitaires Notre-Dame de la Paix: Namur, Belgium, 2001.

29. Rost, M. J.; Crama, L.; Schakel, P.; van Tol, E.; van Velzen-Williams, G. B. E. M.; Overgauw, C. F.; ter Horst, H.; Dekker, H.; Okhuijsen, B.; Seynen, M., et al., Scanning Probe Microscopes Go Video Rate and Beyond. *Rev. Sci. Instrum.* **2005,** *76*, 053710.

30. Leiden Probe Microscopy. http://www.leidenprobemicroscopy.com/ (accessed October 3, 2018).

31. Nečas, D.; Klapetek, P., Gwyddion: An Open-Source Software for Spm Data Analysis. *Open Phys.* **2012,** *10*, 181-188.

32. Assumpção, M. H. M. T.; Piasentin, R. M.; Hammer, P.; De Souza, R. F. B.; Buzzo, G. S.; Santos, M. C.; Spinacé, E. V.; Neto, A. O.; Silva, J. C. M., Oxidation of Ammonia Using Ptrh/C Electrocatalysts: Fuel Cell and Electrochemical Evaluation. *Appl. Catal., B: Env.* **2015,** *174-175*, 136-144.

33. Bergene, E.; Tronstad, O.; Holmen, A., Surface Areas of Pt–Rh Catalyst Gauzes Used for Ammonia Oxidation. *J. Catal.* **1996,** *160*, 141-147.

34. Contour, J. P.; Mouvier, G.; Hoogewys, M.; Leclere, C., X-Ray Photoelectron Spectroscopy and Electron Microscopy of Pt-Rh Gauzes Used for Catalytic Oxidation of Ammonia. *J. Catal.* **1977,** *48*, 217-228.

35. Cowans, B. A.; Jurman, K. A.; Delgass, W. N.; Li, Y. Z.; Reifenberger, R.; Koch, T. A., Scanning Tunneling Microscopy of Platinum-Rhodium Gauze Hcn Catalysts. *J. Catal.* **1990,** *125*, 501-513.

1
2
3
4
5
6
7
8
9
10
11
12
13
14
15
16
17
18
19
20
21
22
23
24
25
26
27
28
29
30
31
32
33
34
35
36
37
38
39
40
41
42
43
44
45
46
47
48
49
50
51
52
53
54
55
56
57
58
59
60

36. Fierro, J. L. G.; Palacios, J. M.; Tomas, F., An Analytical Sem and Xps Study of Platinum–Rhodium Gauzes Used in High Pressure Ammonia Burners. *Surf. Interface Anal.* **1988,** *13*, 25-32.

TOC Graphic